Spectroelectrochemical Evidence of Interconnected Charge and Ion Transfer in Ultrathin Membranes Modulated by a Redox Conducting Polymer

Yujie Liu, Alexander Wiorek, Gaston A. Crespo, and Maria Cuartero*

Cite This: *Anal. Chem.* 2020, 92, 14085−14093

Read Online

ACCESS | Metrics & More | Article Recommendations | SI Supporting Information

ABSTRACT: Previous publications have demonstrated the tuning of ion-transfer (IT) processes across ion-selective membranes (ISMs) with thicknesses in the nanometer order by modulating the oxidation state of a film of a conducting polymer, such as poly(3-octylthiophene) [POT], that is in back-side contact. Attempts on the theoretical description of this charge transfer (CT)−IT system have considered the Nernst equation for the CT, while there is no empirical evidence confirming this behavior. We present herein the first experimental characterization of the CT in POT films involved in different CT−IT systems. We take advantage of the absorbance change in the POT film while being oxidized, to monitor the CT linked to nonassisted and assisted ITs at the sample−ISM interface, from one to three ionophores, therefore promoting a change in the nature and number of the ITs. The CT is visualized as an independent sigmoid in different potential ranges according to the assigned IT. Herein, we have proposed a simple calculation of the empirical CT utilizing the mathematical Sigmoidal−Boltzmann model. The identification of the physical meaning of the mathematical definition of CT opens up new possibilities for the design of sensors with superior analytical features (mainly in terms of selectivity) and the calculation of apparent binding constants in the ISM.
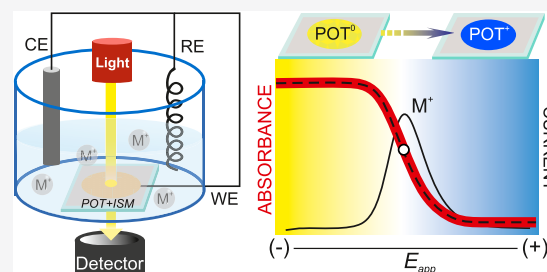
INTRODUCTION

The ion-selective membrane (ISM) is a vivid element of many successful sensing concepts and attracts the attention of different research profiles from fundamental aspects to applied science.[1] On-demand tuning of ion-transfer (IT) processes at the sample−ISM interface has been demonstrated to be a key pathway toward superior analytical features, beyond those provided by traditional potentiometric sensors.[2] Recent efforts have been mainly directed not only toward the use of dynamic electrochemistry (e.g., cyclic voltammetry, CV) as the readout[3−6] but also toward the placement of the sample and electrodes in thin-layer confinements.[7,8]

In the context of ITs exploited as the digitization of ion concentration in the sample, the modulation of ITs across the sample−ISM interface by the charge transfer (CT) in the underlying redox-active film has been recently explored. Our group members have demonstrated vast experience in the use of the conducting polymer poly(3-octylthiophene) (POT) as well as self-assembled monolayers for this purpose.[9−13] Focusing particularly on POT, the gradual oxidation of neutral POT^0 to POT$^+$ is connected to the presence of lipophilic anions in the ISM, e.g., in the cation exchanger tetrakis[3,5-bis(trifluoromethyl)phenyl]borate, Na$^+$TFPB$^−$, that stabilizes the generated positive charge. Then, to maintain the electroneutrality condition, the "hydrophilic" counter-cation (e.g., Na$^+$) is expelled from the membrane to the solution. In other words, the system presents interconnected CT−IT

events (someway) similar to traditional CT−IT processes at polarizable liquid−liquid interfaces.[14−16] These events have to be properly resolved for a complete definition of the working mechanism of the POT−ISM voltammetric system, which is indeed the aim in the present paper.

One peculiarity to be considered is that the ISM is formulated with a reduced thickness (ca. 200 nm calculated by ellipsometry)[17] compared to traditional ISMs used in potentiometry (thickness of hundreds of micrometers).[18] Thus, the system behaves under a thin-layer regime for ion activity in the sample solution higher than $10^{−6}$ M concentration.[19] Accordingly, the Gaussian-shaped voltammetric peak associated with the IT shifts with increasing ion concentration in the sample solution, following the Nernst equation.[9] Furthermore, when multiple receptors (or ionophores) are simultaneously incorporated into the thin ISM, each assisted IT is expressed as a separate peak that independently evolves according to the Nernst equation as a function of the ion concentration (or activity) in the sample.[12] This peak differentiation arises from the distinct ion−
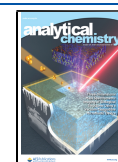
ionophore binding constants and, therefore, the different energies associated with each IT across the ISM. In contrast to traditional potentiometry, multi-ion detection is possible by means of just one measurement with a sole ISE: multi-cation detection was unprecedently demonstrated in a complex matrix such as blood.[17]

Regarding the pure theoretical definition of the working mechanism for such POT–ISM voltammetric electrodes with interconnected CT–IT, essentially, it is assumed that the system is composed of two interfaces corresponding indeed to the CT and the IT events. Then, the potential at each interface is described by the Nernst equation (e.g., eq 1 for the CT), and the generated current was described to be exactly the same in all of the points of the space domain, given by eq 2[9,19]

$$E_{CT} = E_{CT}^0 + \frac{RT}{n_{POT}F} \ln \frac{c_{POT^+}}{c_{POT^0}} \qquad (1)$$

$$i = n_{POT}FA\delta_{POT}\frac{c_{POT^+}}{\partial t} \qquad (2)$$

where E_{CT}^0 is the standard redox potential of the POT oxidation process, R is the gas constant, T is the absolute temperature, n_{POT} is the average number of electrons transferred at the electrode surface from POT^0 to POT^+, A is the active area of the electrode, and δ_{POT} is the thickness of the POT film.

To the best of our knowledge, there is a lack of empirical evidence for using such a Nernst-like description of the CT process in POT in the literature. So far, only the well-known sigmoidal change of the relative conductivity for POT electrodes subjected to cyclic voltammetry (CV) in bulk solution experiments could be attributed to such a definition.[20−22] Some clues for a proper CT definition may indeed arise from the inspection of previous publications. Thus, the POT^0/POT^+ conversion degree was demonstrated to be limited by the amount of $TFPB^-$ in the nanometer-sized ISM; for example, with 40 mmol kg^{-1} NaTFPB, a percentage of ca. 20% of the total available POT^0 participates in the CT–IT.[12] In addition, this process undoubtedly took place at the buried POT–ISM interface.[23] Moreover, it would be crucial to have an analytical technique to precisely follow the dynamic oxidation of the POT film to provide definitive evidence allowing for an unambiguous CT definition.

We present herein the first experimental approach to individually follow the CT in POT films coupled to IT(s) in different ISMs comprising no ionophore, one ionophore (for potassium ion), two ionophores (for lithium and potassium ions), and three ionophores (for lithium, sodium, and potassium ions). We have functionalized regular indium tin oxide (ITO) glass electrodes with a layer of electropolymerized POT and different spin-coated nanometer-sized ISMs on the top. The absorbance change of the POT film is monitored during CV experiments with the mentioned ISMs. Because the absorbance of neutral POT^0 and oxidized POT^+ is different at 450 nm, it is possible to follow the oxidation degree in the POT film simultaneously with the CV experiments by means of spectroelectrochemistry. Thus, we mathematically analyze the working mechanism of voltammetric thin membranes comprising different numbers of ionophores on the basis of new experimental insights into the CT process. The proposed methodology may be extrapolated to any other redox-active film involving changes in its optical properties (also

fluorescence) when in contact with any kind of ISM or organic film/phase with ion-exchange properties.

EXPERIMENTAL DETAILS

The ITO-coated glass electrodes were cleaned with ethanol by ultrasonification and then rinsed with water. During POT synthesis, a solution containing 0.1 M concentration of 3-octylthiophene and LiClO$_4$ in acetonitrile (ACN) was used. After degassing by purging with nitrogen for 15 min, POT was electrochemically polymerized on the ITO electrode by performing cyclic voltammetry (0−1.5 V, 100 mV s^{-1}, 2 scans) and then discharged at 0 V for 120 s. A platinum electrode and a homemade Ag/AgCl wire were used as the counter and the reference electrode, respectively, in the three-electrode cell. Thereafter, the synthesized POT film was immersed in ACN and then tetrahydrofuran (THF) for 30 min and 10 s, respectively. Stock membrane cocktails were prepared according to the compositions presented in Table S1. Then, the cocktails were diluted in THF: 50 μL of stock membrane cocktail + 150 μL of THF. A volume of 30 μL of diluted membrane cocktail was deposited on the POT-based ITO by spin coating (1500 rpm, 60 s) using a spin-coater provided by GreatCell Solar (Australia). The spectroelectrochemical cell was prepared as reported elsewhere.[24] The POT film was illuminated from the top of the electrochemical cell, and the transmitted light was collected at the bottom after absorption by the modified ITO. Notably, the same cell was used for POT electropolymerization. During CV experiments, the spectra of the POT film were collected with an acquisition time of 120 ms. Three spectra were averaged to improve the signal-to-noise ratio. For more experimental details, the reader is referred to the Supporting Information.

RESULTS AND DISCUSSION

Spectroelectrochemistry is herein introduced to investigate the role of POT assisting different IT processes across nanometer-sized ISMs with an increasing number of ionophores. We aim at demonstrating for the first time how the nature and number of ITs occurring at the sample−ISM interface dictate the dynamic POT^+/POT^0 conversion. While the ITO−POT−ISM electrode is polarized with anodic linear sweep potential, the absorption of the POT film at a selected wavelength is continuously monitored: a dynamic change in absorbance is expected to occur as the POT^+/POT^0 conversion degree progresses in the film. This is supported by previous studies reporting a change in POT and also other thiophene-based conducting polymers' spectra at increasing (individual) polarization potentials.[21,25−27]

Figure 1a displays the absorption spectra of the POT film under three different conditions: the nonpolarized film (tested immediately after POT electropolymerization with a film providing a constant open-circuit potential of 343.7 ± 4.0 mV for 30 min in 0.1 M TBAPF$_6$/ACN solution), the film polarized at 0 V, and the film polarized at 1.4 V. The spectrum of the nonpolarized film and that of the film polarized at 0 V is essentially the same, showing a well-defined band at ca. 450 nm assigned to $\pi \rightarrow \pi^*$ electron transitions in the reduced (or neutral) POT^0.[21] This band is almost imperceptible in the spectrum of the film polarized at 1.4 V, with one broad band being intuited from 1000 nm that corresponds to $\pi \rightarrow$ polaron transitions in oxidized POT^+.[22] At 450 nm, it is possible to distinguish between POT^0 and POT^+ by the disappearance of
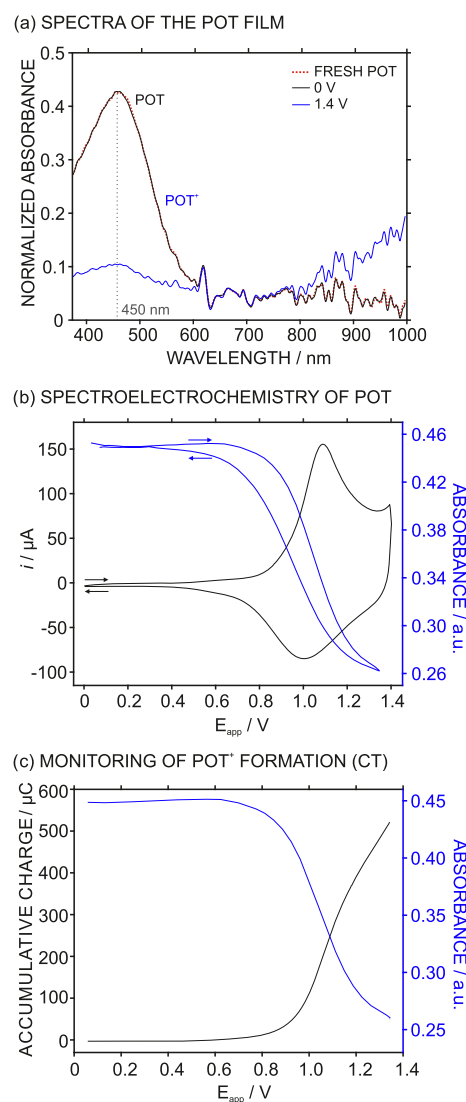
Figure 1. (a) Spectra of the POT film: nonpolarized, polarized at 0 V, and polarized at 1.4 V. (b) Spectroelectrochemistry in the POT film. CV at 100 mV s^{-1} and absorbance registered at λ = 450 nm. (c) Correspondence of the dynamic integrated charge under the anodic peak (coulovoltagram) with the dynamic absorption of the POT film. All of the experiments were performed in 0.1 M TBAPF$_6$/ACN solution.

the described absorbance band. Once the possibility of distinguishing between the POT^0 and POT$^+$ state at 450 nm was confirmed, a possible relation between the POT$^+$/POT^0 degree in the film and the acquired absorbance was investigated again using spectroelectrochemistry.

Figure 1b presents the interrogation of the POT film using CV in 0.1 M TBAPF$_6$/ACN solution while monitoring its absorption. During the anodic scan, POT^0 is oxidized to POT$^+$ and doped with PF$_6^-$ ions in the solution. This is seen in a voltammetric peak at ca. 1.1 V, coinciding with a decrease in the dynamic absorbance. The opposite trend occurs during the cathodic scan. The sigmoidal shape observed in the dynamic absorbance (absorbance versus $E_{app}(t)$) for both the anodic and cathodic scans is evident and indeed reproducible during successive CVs (Figure S1 and Table S2). It must be noticed that henceforth only the anodic part of any CV is considered in

our discussions for simplicity; evidently, the same interpretation can be applied to the cathodic scan for the reverse process.

Next, we investigate whether there exists any useful relationship between the POT$^+$/POT^0 conversion and the dynamic absorbance. For this purpose, the anodic voltammetric peak was transformed into the corresponding coulovoltagram (i.e., dynamic accumulative charge while increasing the applied potential as a result of the integration of the voltammetric peak),[23] as presented in Figure 1c. As observed, the coulovoltagram also displayed a sigmoidal shape in which the initiation of the horizontal asymptote rather coincides with that in the absorbance curve, and then the accumulative charge increases as the absorbance decreases, implying in both cases the formation of POT$^+$. The final asymptote was not reached in any case but is intuited, likely because of the capacitive current shown at the end of the voltammetric peak impeding/masking the total oxidation of the POT film. Furthermore, from ca. 0.9 to 1.3 V, there is a linear relationship between the integrated charge (and therefore the amount of oxidized POT$^+$) and the absorbance as follows: (Q (μC) = [$-2823.9 \cdot$absorbance (au)] + 1158.5, r^2 = 0.998), addressing the expected liaison in the spectroelectrochemistry experiments.

We then proceeded with the evaluation of the POT oxidation process when coupled to different ITs across thin ISMs. Several membranes were tested by depositing them on top of the POT film: M1 without any ionophore, M2 with one ionophore (for potassium), M3 with two ionophores (for lithium and potassium), and M4 with three ionophores (for lithium, sodium, and potassium); see Table S1. The number of selective ITs was increased (i.e., from none in M1 to three in M4), while always ensuring the availability of the peak for the transfer of potassium ion (K$^+$) as a reference.

As detailed in the Introduction section, once POT is covered by a thin ISM, the generated POT$^+$ during the anodic potential sweep is paired (and stabilized) by TFPB$^-$ and the remaining Na$^+$ is expelled to the solution to maintain electroneutrality. Then, because POT oxidation is connected to the cation-transfer phenomenon at the sample−ISM interface, we expect to observe different curves in the dynamic absorbance of POT for the different membranes. Figure 2 depicts the cyclic voltammetric curves for M1−M4 with the corresponding dynamic absorbance. It is worth mentioning that control experiments with all of the membranes without a POT film at the back-side revealed a constant absorbance over 15 subsequent CVs (average deviation of ± 0.001 absorbance units), confirming that any change in absorbance in the ITO−POT−ISM electrode is purely due to intrinsic absorption changes in POT.

Whether the thin ISM contains no ionophore and only one cation is present in the sample solution, only one IT is feasible, which is well-represented by a reversible wave at 0.4 V in the voltammogram in Figure 2a (M1 in KCl solution: K$^+$ transfer across the sample−ISM interface). The anodic peak is developed from ca. 0 to 0.65 V, coinciding with the sigmoidal-shaped decrease in the dynamic absorbance of the POT film. An analogous peak was shown by membrane M2 (Figure 2b) shifting to more positive potentials (ca. 0.9 V for the anodic peak) and being rather narrower (width at the half peak of 90 mV in M2 versus 280 mV in M1), as a consequence of the presence of the ionophore. Notably, any difference displayed in the peak current when membranes M1 and M2 are compared (i.e., 15 versus 12 μA in Figure 2a,b) arises from
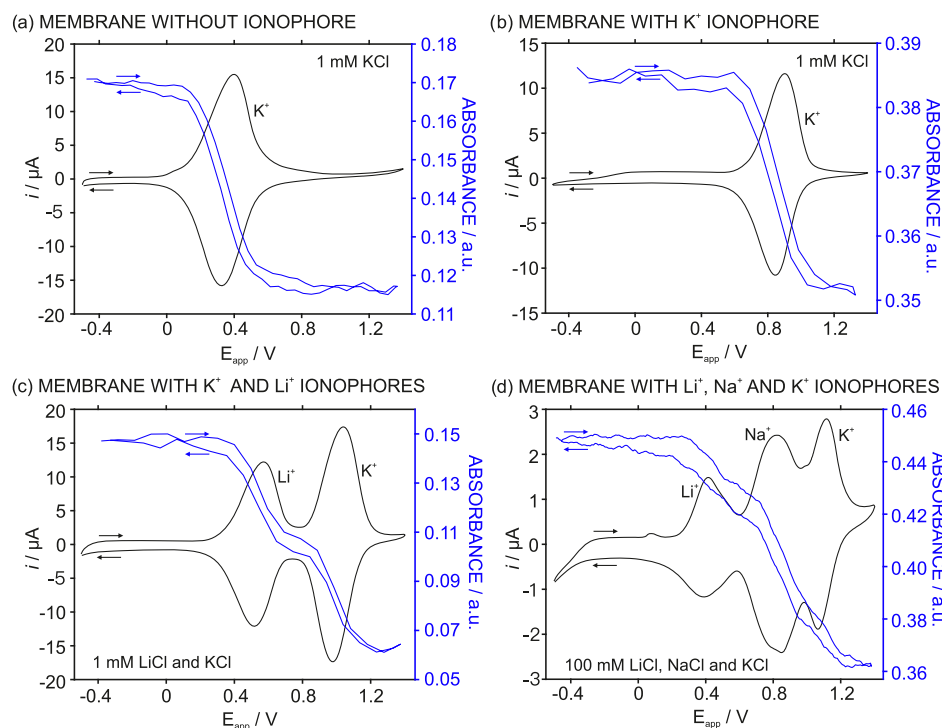
Figure 2. CVs and the associated dynamic absorbance for different membrane-based systems: (a) M1 without ionophore in 1 mM KCl, (b) M2 with potassium ionophore in 1 mM KCl/10 mM NaCl background solution, (c) M3 with lithium and potassium ionophores in 1 mM LiCl / 1 mM KCl / 10 mM NaCl background solution, and (d) M4 with lithium, sodium, and potassium ionophores in 100 mM LiCl/100 mM NaCl/100 mM KCl/100 mM MgCl$_2$ background solution. A scan rate of 100 mV s^{-1} was used for M1−M3 and a scan rate of 25 mV s^{-1} was used for M4.

variability in the electrode fabrication rather than (electro)-chemical reasons, as also noticed in previous studies.[9]

When membrane M2 is immersed in the sample solution, all of the Na$^+$ ions initially present in the membrane (provided by NaTFPB) are immediately replaced by K$^+$ in the solution because of the high selectivity of the ionophore toward this cation and the existing concentration gradient. The spontaneous depletion or extraction of the primary ion analyte into an ionophore-based ISM is calculated to be a very rapid process, taking around 20 ms for a film thickness of 200 nm, and with a diffusion coefficient of 10^{-8} cm^2 s^{-1}.[9,28] Then, K$^+$ is complexed by the ionophore in the membrane, resulting in a higher energy requirement to promote its release during POT^0 oxidation, which translates to a higher peak potential. In addition, the sigmoidal change in the dynamic absorption spectrum related to POT^0−POT$^+$ transition similarly shifts to higher potentials. Thus, the potential range in which POT^0 oxidation occurs is exclusively dictated by the required energy associated with the connected IT at the sample−ISM interface. This is indeed herein demonstrated for the first time, owing to the individualization of the POT^0/POT$^+$ dynamic conversion through spectroelectrochemistry experimental measurements.

In the case of two ionophores and the sample solution containing an equal concentration of the two cations for which the membrane is selective, the CV displayed two waves related to the transfer of these two cations. The wave appearing at the first place in the anodic scan corresponds to the cation less preferred by the membrane or, in other words, the lower cation−ionophore binding constant in the membrane. Specifically for Li$^+$ and K$^+$ (membrane M3, Figure 2c), it is expected that the peak for Li$^+$ appears at the first place (0.68 V) because of the lower binding constant (log β of 4.37 for Li$^+$ against 10.10 for K$^+$) and then the peak for K$^+$ appears at more

positive potentials (1.1 V).[29] We have already demonstrated this peak attribution in a previous study based on multi-ionophore thin membranes.[12] Regarding the associated dynamic absorbance, there is a transition in the curve from ca. 0.75 to 0.8 V, coinciding with the changeover region between the two voltammetric peaks. The absorbance curve is divided into two different parts related to the two cation transfers occurring at the sample−membrane interface. Between the two transfers, the absorbance became significantly constant because the POT film was not oxidized (no CT process), given that there is no connected cation transfer−IT process energetically available in this potential region (i.e., from 0.75 to 0.8 V).

The curve for the dynamic absorbance is the same at different scan rates (see Figure S2). As a result, the evolution of the POT$^+$/POT^0 degree during the voltammetric scan is independent of the speed of the applied potential. This behavior is, in principle, expected, as the charge under the voltammetric peak is known to be independent of the scan rate,[9] i.e., again a demonstration that CT and IT processes are fully interconnected. Advantageously, a lower scan rate provides longer analysis time that allows for a higher amount of the acquired data in the optical measurements and, therefore, the described transition between Li$^+$ and K$^+$ transfers is slightly better defined (Figure S3). Whatever the scan rate, the dynamic absorbance and described transition are totally reproducible in subsequent voltammetric scans, as shown in Figure S4a and Table S2. Good reproducibility was also displayed by the previous membranes M1 and M2 (Figure S4b,c and Table S2).

Figure 2d presents the CV and the corresponding dynamic absorbance of the POT film coupled to membrane M4, which contains three ionophores for lithium, sodium, and potassium.

Notably, the scan rate in this experiment was 25 mV s^{-1}, much lower than that in the previous membranes (100 mV s^{-1}), attempting to reach a great level of definition of the dynamic absorbance profile with significant overlapping conditions of the voltammetric peaks. As observed, three voltammetric waves appeared, the first peak at 0.4 V corresponds to Li$^+$, the second one at 0.8 V to Na$^+$, and the last peak at 1.15 V was assigned to K$^+$, as per the order of the binding constants with the corresponding ionophores (log β of 4.37, 7.69, and 10.10, respectively). The same peak assignment has already been demonstrated for a similar membrane in our previous work.[12] In the dynamic absorbance, three different sigmoidal-shaped regions can be distinguished, coinciding with each voltammetric peak. Between each region, almost no change in the absorbance was displayed (i.e., from 0.5 to 0.7 V and from 0.9 to 1.0 V). While the transitions between each cation transfer can be in fact distinguished, these are less evident than those in membrane M3 with only two ionophores. This is probably due to an increase in the overlapping of the voltammetric peaks or ITs.

To further inspect the results obtained with membranes M1−M4, the corresponding dynamic absorbance plots and the coulovoltagrams from the anodic scans were normalized and are displayed in Figure 3. Notably, the normalization allows for

Figure 3. (a) Normalized absorbance for POT with M1−M4. (b) Normalized charge (accumulative charge integrated under the voltammetric peak) for POT with M1−M4. CT = charge transfer. IT = ion transfer.

normalized absorbance (Figure 3a), a decrease following a sigmoidal-shaped curve was evident, reflecting the conversion of POT^0 to POT$^+$, in other words, the description of the CT in the system. However, this decrease is different depending on the nature and number of the cation transfers at the sample−membrane interface. Thus, comparing nonassisted (NAS)- and ionophore-assisted (AS) ITs, the potential range in which the sigmoidal decrease is displayed shifts to more positive values. As an example, the reader is referred to the experimental curves in KCl for membranes M1 and M2 with the inflection point of the sigmoid shifting from 360 to 860 mV.

The sigmoidal decrease is now divided into different regions, displaying individual sigmoidal curves for every cation transfer. The membrane based on two ionophores (M3) showed two regions, and the membrane with three ionophores (M4) displayed three regions. Importantly, the position for each individual curve (i.e., the inflection point of each individual sigmoid) depends on the associated peak position in the voltammogram, i.e., the energy associated with each IT. The different regions are less evident in the dynamic absorbance profile, depending on the overlapping degree between the voltammetric peaks. The results in Figure 3a also demonstrated that the less responsive regions in the dynamic absorbance profile coincide with the transitions between the different cation transfers. At these potential windows, the CT does not occur in POT because there is no connected IT to maintain electroneutrality in the process.

The coulovoltagrams in Figure 3b displayed the same trends as those for the dynamic absorbance but for the increasing accumulative charge related to (or including) the IT. Indeed, we attempted to correlate the position (inflection point) of every individual sigmoid found in the dynamic absorbances and coulovoltagrams, as shown in Table 1. There is an evident
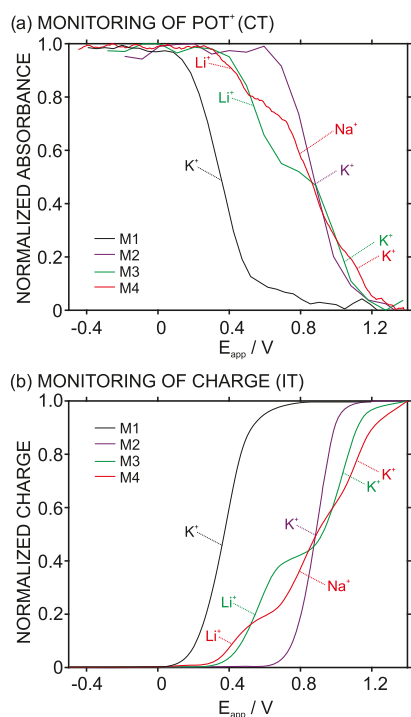
Table 1. Parameters for the Dynamic Absorbance (CT in POT), the Coulovoltagram (Coulovolt), and the Associated Anodic Peak in CV

		sigmoidal change(s) (from−to, mV)		inflection point(s) (mV)		
		CT	coulovolt	CT	coulovolt	peak (mV)
M1	K$^+$	43−872	43−855	360	382	399
M2	K$^+$	595−1180	585−1177	860	889	902
M3	Li$^+$	224−692	231−715	544	543	568
	K$^+$	840−1278	865−1204	990	1033	1039
M4	Li$^+$	248−551	221−553	430	431	414
	Na$^+$	590−1009	617−1016	843	824	821
	K$^+$	1058−1224	1034−1241	1136	1121	1119

a better comparison of all of the ISMs together because each membrane was prepared with a different amount of NaTFPB to promote all of the possible ITs according to an increasing number of ionophores in the membrane (Table S1). In addition, the higher the number of ionophores in the membrane, the higher the amount of NaTFPB needed for this purpose, and, as a result, more POT^0 is oxidized to POT$^+$ and more absorbance change is obtained.[12] Inspecting then the

agreement between the potential range in which the sigmoidal change occurs in the CT and charge development in the coulovoltagram. In addition, the inflection point in both sigmoid curves for each system not only coincides between them but also with the anodic peak potential in the raw CV. The largest difference was found for the K$^+$ peak in membrane M3 (43 and 49 mV difference between the inflection points and the peak position, respectively, representing ca. 4% of the total potential magnitude). Even in this case, an agreement of the results may also be considered owing to the small variance. Most probably, faster acquisition time in dynamic absorbance would help in the improvement of the closeness of these parameters. However, the compliance is rather evident and

indeed confirmed by the linear relationship found between the integrated charge and the absorbance for all of the membranes tested (see Figure S5). Again, this trend shows the absolute relationship between the development of the CT process in the POT film and its inherent connection to the IT occurring at the membrane−sample interface.

Subsequently, we simulated the dynamic absorbance plots and the coulovoltagrams for systems based on M1−M4 using a theoretical fitting to the mathematical Sigmoidal−Boltzmann model, according to eqs 3−5, respectively

$$Y = A_2 + \frac{A_1 - A_2}{1 + e^{(x - x_0/k)}} \tag{3}$$

$$Y = A_3 + \frac{A_1 - A_2}{1 + e^{(x - x_0/k)}} + \frac{A_2 - A_3}{1 + e^{(x - x_0'/k')}} \tag{4}$$

$$Y = A_4 + \frac{A_1 - A_2}{1 + e^{(x - x_0/k)}} + \frac{A_2 - A_3}{1 + e^{(x - x_0'/k')}} \\ + \frac{A_3 - A_4}{1 + e^{(x - x_0''/k'')}} \tag{5}$$

where A_1, A_2, A_3, and A_4; x_0, x_0', and x_0''; and k, k', and k'' are parameters to be adjusted. x is fixed as the applied potential during the anodic scan and Y is the normalized absorbance or normalized charge (dimensionless). Figure 4 shows the overlapping of the experimental and calculated curves, whereas Table 2 collects the parameters used for the theoretical simulations. Note that the direction of the normalized charge was inverted in the following plots for rather appropriate comparison with the normalized absorbance, but the parameters for the theoretical simulations were used as per the increasing sigmoid. Experimental and calculated curves rather coincide in all of the cases, even for the membrane with three ionophores (M4), presenting a higher degree of overlap between the ITs. This excellent correlation confirms the validity of the mathematical Sigmoidal−Boltzmann model to describe the studied CT−IT processes.

Relevant information about the CT in POT is obtained after a deep inspection of Table 2, together with the assumption that the CT can be described by the Nernst equation, as previously suggested in the literature. This allows for the physical interpretation of the parameters in the mathematical Sigmoidal−Boltzmann model. From eq 1, it is possible to easily obtain a sigmoidal-like equation considering that the total concentration of POT (c_{POT}) is always equal to the sum of the neutral (c_{POT^0}) and the oxidized (c_{POT^+}) forms coexisting in the film

$$c_{POT} = c_{POT^0} + c_{POT^+} \tag{6}$$

This sigmoidal-like equation is as follows (see the Supporting Information for more details on its development)

$$\frac{c_{POT^0}}{c_{POT}} = \frac{1}{1 + e^{(E_{CT} - E_{CT}^0)n_{POT}F/RT}} \tag{7}$$

Evidently, eqs 3 and 7 coincide if

$$Y = c_{POT}/c_{POT^0} \tag{8}$$

$$A_2 = 0 \tag{9}$$

$$A_1 - A_2 = 1 \text{ and therefore, } A_1 = 1 \tag{10}$$

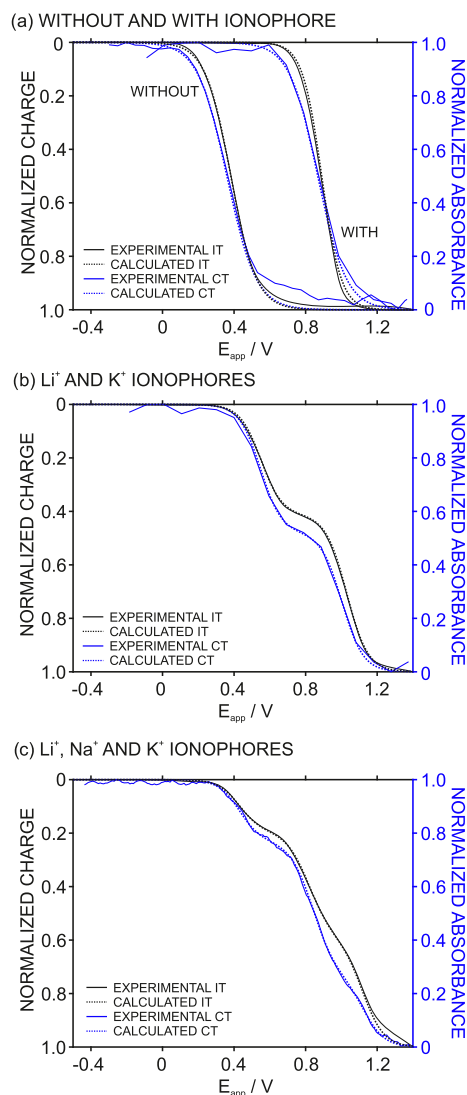$$x - x_0 = E_{CT} - E_{CT}^0 \tag{11}$$

Figure 4. Theoretical normalized charge in coulovoltagrams (linked to IT) and normalized absorbance (linked to CT) observed in systems with (a) M1 and M2 using eq 3, (b) M3 using eq 4, and (c) M4 using eq 5. The displayed experiments correspond to the CVs and dynamic absorbance shown in Figure 2.

and

$$1/k = n_{POT}F/R\ T \tag{12}$$

As a result, k represents the slope of the Nernst equation related to the CT process, whereas A_1 and A_2 reflect the conversion of POT between 0 and 1 (normalized to the maximum and minimum amount to be oxidized). This reasoning is also valid for the CT in POT films coupled to membrane M1 (without ionophore) or M2 (with potassium ionophore), which follows eq 3. In particular, these two membranes displayed $A_1 = 1$ and $A_2 = 0$, coinciding with the expected values for a Nernstian-described process, $x_0 = 360$ and 860 mV, in agreement with the peak potentials (see Table 2), and k should correspond to the Nernstian slope, being slightly higher than the theoretical value of 0.059 V in the case of membrane M1.

Inspecting the calculated coulovoltagrams of these two membranes, which involved the IT processes, a similar translation as that for the CT is realized. However, this time

Table 2. Parameters Used for the Theoretical Simulations in Membranes M1−M4

	A values		*x*$_0$ values (V)		*k* values (V)	
	CT	coulovolt	CT	coulovolt	CT	coulovolt
M1	A_1: 1	A_1: 0	x_0: 0.36	x_0: 0.38	k: 0.081	k: 0.071
	A_2: 0	A_2: 1				
M2	A_1: 1	A_1: 0	x_0: 0.86	x_0: 0.89	k: 0.054	k: 0.054
	A_2: 0	A_2: 1				
M3	A_1: 1	A_1: 0	x_0: 0.54	x_0: 0.55	k: 0.059	k: 0.059
	A_2: 0.52	A_2: 0.41	x_0': 0.99	x_0': 1.03	k': 0.059	k': 0.059
	A_3: 0	A_3: 1				
M4	A_1: 1	A_1: 0	x_0: 0.43	x_0: 0.43	k: 0.059	k: 0.059
	A_2: 0.77	A_2: 0.19	x_0': 0.84	x_0': 0.82	k': 0.065	k': 0.065
	A_3: 0.26	A_3: 0.60	x_0'': 1.13	x_0'': 1.12	k'': 0.059	k'': 0.059
	A_4: 0	A_4: 1				

A_1 is equal to 0 and A_2 is equal to 1, thereby defining an increasing sigmoid; x_0 and k have rather similar values for both fittings: the CT in POT and the coulovoltagram (see Table 2).

Regarding membranes with more than one ionophore (M3 and M4), the interpretation of the fitting parameters of the Sigmoidal−Boltzmann model in relation to the Nernstian description of the processes is rather straight forward, despite the complexity added to the system. Thus, A_1 is equal to 1, and the last A value (i.e., A_3 for M3 and A_4 for M4) is equal to 0. Then, intermediate A values are related to the transition between the different IT processes. For example, in membrane M3 displaying two ITs for Li$^+$ and K$^+$, A_2 is close to 0.5 (see Table 2), which means that the transition between the two ITs occurs in the middle of the sigmoid.

For membrane M4, if we consider that the entire CT is divided into three ITs with a similar charge distribution, A_2 and A_3 are expected to be 0.7 and 0.3, respectively, indeed very close to the values presented in Table 2. Considering now the physical meaning of A as the conversion degree of POT between 0 and 1 (normalized to the maximum and minimum amount to be oxidized), it is evident from the theoretical A values that the amount of POT^0 oxidized to POT$^+$ is equally distributed between all of the ITs possible in each membrane. This is indeed a really valuable discovery concerning the definition of the entire CT−IT system. Then, the calculated x_0 values for both membranes (M3 and M4) coincide again with the peak position for each IT in the experimental voltammogram, comparing Tables 1 and 2. Furthermore, the slopes perfectly agree with Nernstian behavior.

Additional use of the proposed mathematical model arises when considering the thermodynamic correlation between the peak position in experimental CVs corresponding to NAS or AS extraction of ions from the solution and different membranes, as previously suggested for CT−IT processes.[12] The Nernst equation is used to define NAS and AS processes as follows

$$(E_{IT})_{NAS} = (E_{IT}^0)_{NAS} + \frac{RT}{n_{IT}F} \ln \frac{c_I^{aq}}{c_I^{org}} \tag{13}$$

$$(E_{IT})_{AS} = (E_{IT}^0)_{AS} + \frac{RT}{n_{IT}F} \ln \frac{c_L^{org} c_I^{aq}}{c_{I-L}^{org}} \tag{14}$$

where I represents a general cation, aq refers to the aqueous phase (sample), and org refers to the organic phase (membrane). Equation 14 can be expressed in terms of the cation−ionophore binding constant (β_{I-L}) as follows

$$\beta_{I-L} = c_{I-L}^{org}/c_I^{org}c_L^{org} \tag{15}$$

$$(E_{IT} - E_{IT}^0)_{AS} = \left(S \log \frac{c_I^{aq}}{c_I^{org}} \right) - (S \log \beta_{I-L}) \tag{16}$$

where $S = RT/2.3n_{IT}F$. Then, inserting eq 13 in eq 16, and assuming equal concentrations of I in the aqueous phase in both NAS and AS processes, the following relationship is obtained

$$\log \beta_{I-L} = \frac{(E_{IT} - E_{IT}^0)_{NAS} - (E_{IT} - E_{IT}^0)_{AS}}{S} \tag{17}$$

Considering our spectroelectrochemistry experiments, all of the parameters in eq 17 can be obtained from either the CV, dynamic absorbance related to the CT in POT, or the coulovoltagram calculations. In this particular case, the potential is externally controlled by the application of an anodic linear sweep protocol, and E_{IT} is assumed to be equal in both NAS and AS transfers. As a result, eq 17 is rewritten as follows

$$\log \beta_{I-L} = \frac{(E_{IT}^0)_{AS} - (E_{IT}^0)_{NAS}}{S} \tag{18}$$

with E_{IT}^0 values coinciding not only with the peak potential of anodic peaks for the same concentration of the ion using membranes with and without the ionophore under study but also to x_0 values in the mathematical calculations.

In the case of 10 mM K$^+$ measured with membranes M1 and M2, i.e., with and without valinomycin as an ionophore, the peak potentials were found to be 399.2 and 926.2 mV, respectively. Then, according to eq 18 and considering that both membranes present an ideal Nernstian behavior (i.e., S = 59.2 mV), the binding constant $\log \beta_{K\text{-valinomycin}}$ is calculated to be 8.9. This value rather agrees with those previously reported in the literature for DOS-based membranes, utilizing different calculation approaches: segmented sandwich membranes (values of 10.10[29] and 10.00[30]), a two-ionophore protocol (8.32[31]), and thin-voltammetric membranes (9.49[12]). Interestingly, the calculated $\log \beta_{K\text{-valinomycin}}$ indeed becomes even closer in value to those previously reported if x_0 and k values for the calculated CT and coulovoltagram (Table 2) are considered: $\log \beta_{K\text{-valinomycin}}$ = (0.86 − 0.36)/(0.054) with a value of 9.26 and $\log \beta_{K\text{-valinomycin}}$ = (0.89 − 0.38)/(0.054) with a value of 9.44, respectively.

These promising results open up new avenues in the direction of validating the spectroelectrochemical methodology

with massive experiments based on different ion−ionophore systems. The final purpose would be to propose a reliable alternative to the traditional (and tedious) segmented sandwich method.[30] Moreover, investigations may be extended to the calculation of selectivity constants in nanometer-sized membranes, including cross-selectivity in multi-ionophore-based membranes, which has no precedents to date.

Finally, we explored the evolution of the dynamic absorbance of the POT film at increasing concentrations of the cation analyte(s) in the sample solution. As expected, the voltammetric peaks observed in membranes M2 and M3 shifted to more positive potentials, according to the Nernstian behavior.[12] As an example, Figure S6 depicts the voltammograms for M2 at increasing concentrations of K^+ and the corresponding calibration graph. The same shift was observed for the related dynamic absorbance in both membranes, as depicted in Figure 5. Regarding membrane M2, a linear relationship was found from 10^{-4} to 10^{-1} M between the

logarithmic activity of K^+ in the sample and the potential at which the inflection point appeared in the sigmoid (see Figure 5c). This correlation was also displayed by membrane M3 based on two ionophores (i.e., considering the second part of the sigmoid), with the particularity of a narrower linear range (from 10^{-3} to 10^{-1} M) most likely due to the overlapping with Li^+ transfer (i.e., cross-selectivity). Evidently, a linear correlation is also expected for Li^+ (i.e., the first part of the sigmoid), but this seems to occur only at higher Li^+ concentrations (from 10^{-2} to 10^{-1} M). However, the evolution of the dynamic absorbance for a single sigmoid in NaCl background (dotted line) to a curve based on two sigmoid portions for the main cation transfers across the membrane is clear (see Figure 5b). Overall, the linear correlations found with the concentration of the cation(s) analyte(s) on the basis of the newly proposed spectroelectrochemical experiments deserve special attention for further analytical purposes. A deep optimization of membrane thickness, scan rate in the applied potential, and frequency acquisition of the optical measurements would contribute to a fine-tuning of the obtained linearity.

■ CONCLUSIONS

Spectroelectrochemistry has provided the very first experimental evidence on CT dynamic progress in POT films exclusively coupled to IT processes. The advantage of the method is the isolation of the CT owing to the optical readout while stimulating the IT through the application of linear sweep potential. The CT is expressed in a sigmoid coinciding with the range of the applied potential in which the IT occurs. If more than one IT is possible, the entire sigmoid curve is divided into portions (also with a sigmoid shape) linked to each IT. Between the ITs, the experiments demonstrate that no POT is oxidized because no IT occurs. These results advantageously go beyond the traditional definition of CT into CT−IT systems, which, to date, consider that POT is oxidized through a unique (and continuous) process in the entire linear sweep potential. Experimental data for CT connected to multiple ITs perfectly fit the mathematical Sigmoidal−Boltzmann model, allowing for a clear correlation with physical parameters, such as voltammetric peak potential, Nernstian slope, and the normalized degree of oxidized POT. Besides the unquestionable value of these findings toward a reliable theoretical definition of any CT−IT system, the developed approach serves for the easy calculation of thermodynamic parameters (such as ion−ionophore binding constants).

■ ASSOCIATED CONTENT

ⓢ Supporting Information

The Supporting Information is available free of charge at https://pubs.acs.org/doi/10.1021/acs.analchem.0c03124.

> Subsequent measurements of dynamic absorbance of the POT film; influence of the scan rate; additional voltammograms; and equation development (PDF)

■ AUTHOR INFORMATION

Corresponding Author

  Maria Cuartero − *Department of Chemistry, School of Engineering Sciences in Chemistry, Biotechnology and Health, KTH Royal Institute of Technology, SE-100 44 Stockholm, Sweden;* ⓞ orcid.org/0000-0002-3858-8466; Email: mariacb@kth.se
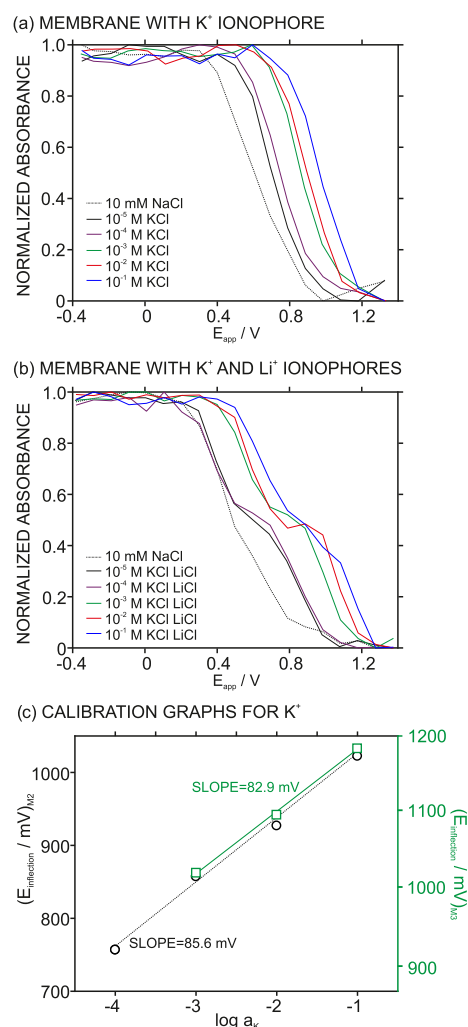
Figure 5. Normalized absorbance at increasing concentrations of the cation(s) analyte(s) in the sample solution. (a) Membrane M2 with potassium ionophore. (b) Membrane M3 with potassium and lithium ionophores. (c) Linear correlations between the logarithmic potassium activity and the inflection point of the corresponding sigmoid in the dynamic absorbance of the POT film in contact with M2 (black) and M3 (green). The scan rate of the corresponding CVs = 100 mV s^{-1}.

Authors

Yujie Liu − *Department of Chemistry, School of Engineering Sciences in Chemistry, Biotechnology and Health, KTH Royal Institute of Technology, SE-100 44 Stockholm, Sweden*

Alexander Wiorek − *Department of Chemistry, School of Engineering Sciences in Chemistry, Biotechnology and Health, KTH Royal Institute of Technology, SE-100 44 Stockholm, Sweden*

Gaston A. Crespo − *Department of Chemistry, School of Engineering Sciences in Chemistry, Biotechnology and Health, KTH Royal Institute of Technology, SE-100 44 Stockholm, Sweden;* orcid.org/0000-0002-1221-3906

Complete contact information is available at:
https://pubs.acs.org/10.1021/acs.analchem.0c03124

Notes

The authors declare no competing financial interest.

REFERENCES

(1) Jackson, D. T.; Nelson, P. N. *J. Mol. Struct.* **2019**, *1182*, 241−259.

(2) Bakker, E. *Anal. Chem.* **2016**, *88*, 395−413.

(3) Si, P. C.; Bakker, E. *Chem. Commun.* **2009**, *35*, 5260−5262.

(4) Kim, Y.; Amemiya, S. *Anal. Chem.* **2008**, *80*, 6056−6065.

(5) Zhang, J.; Harris, A. R.; Cattrall, R. W.; Bond, A. M. *Anal. Chem.* **2010**, *82*, 1624−1633.

(6) Vanamo, U.; Hupa, E.; Yrjana, V.; Bobacka, J. *Anal. Chem.* **2016**, *88*, 4369−4374.

(7) Cuartero, M.; Crespo, G. A.; Bakker, E. *Chimia* **2015**, *69*, 203−206.

(8) Cuartero, M.; Crespo, G. A.; Afshar, M. G.; Bakker, E. *Anal. Chem.* **2014**, *86*, 11387−11395.

(9) Crespo, G. A.; Cuartero, M.; Bakker, E. *Anal. Chem.* **2015**, *87*, 7729−7737.

(10) Cuartero, M.; Chai, L. J.; Zhang, B. B.; De Marco, R.; Crespo, G. A. *Electrochim. Acta* **2019**, *315*, 84−93.

(11) Xu, K. Q.; Cuartero, M.; Crespo, G. A. *Sens. Actuators, B* **2019**, *297*, No. 126781.

(12) Cuartero, M.; Crespo, G. A.; Bakker, E. *Anal. Chem.* **2016**, *88*, 1654−1660.

(13) Yang, Y.; Cuartero, M.; Goncales, V. R.; Gooding, J. J.; Bakker, E. *Angew. Chem., Int. Ed.* **2018**, *57*, 16801−16805.

(14) Zhou, M.; Gan, S. Y.; Zhong, L. J.; Dong, X. D.; Ulstrup, J.; Han, D. X.; Niu, L. *Phys. Chem. Chem. Phys.* **2012**, *14*, 3659−3668.

(15) Zanotto, F. M.; Fernandez, R. A.; Dassie, S. A. *Electrochim. Acta* **2017**, *258*, 727−734.

(16) Gschwend, G. C.; Olaya, A.; Peljo, P.; Girault, H. H. *Curr. Opin. Electrochem.* **2020**, *19*, 137−143.

(17) Cuartero, M.; Crespo, G. A.; Bakker, E. *Anal. Chem.* **2016**, *88*, 5649−5654.

(18) Zdrachek, E.; Bakker, E. *Anal. Chem.* **2019**, *91*, 2−26.

(19) Yuan, D. J.; Cuartero, M.; Crespo, G. A.; Bakker, E. *Anal. Chem.* **2017**, *89*, 586−594.

(20) Rahaman, M.; Aldalbahi, A.; Govindasami, P.; Khanam, N.; Bhandari, S.; Feng, P.; Altalhi, T. *Polymers* **2017**, *9*, 527.

(21) Kondratiev, V. V.; Kurdakova, V. V.; Antonov, N. G.; Tolstopyatova, E. G. *Russ. J. Electrochem.* **2008**, *44*, 286−292.

(22) Palacios, R. E.; Barbara, P. F. *J. Fluoresc.* **2007**, *17*, 749−757.

(23) Cuartero, M.; Acres, R. G.; De Marco, R.; Bakker, E.; Crespo, G. A. *Anal. Chem.* **2016**, *88*, 6939−6946.

(24) Wiorek, A.; Cuartero, M.; De Marco, R.; Crespo, G. A. *Anal. Chem.* **2019**, *91*, 14951−14959.

(25) Trznadel, M.; Zagorska, M.; Lapkowski, M.; Louarn, G.; Lefrant, S.; Pron, A. *J. Chem. Soc., Faraday Trans.* **1996**, *92*, 1387−1393.

(26) Jang, S. Y.; Sotzing, G. A.; Marquez, M. *Macromolecules* **2002**, *35*, 7293−7300.

(27) Jang, S. W.; Yuan, H.; Kim, D. E.; Kim, K. J.; Kang, B. H.; Eum, N. S.; Kang, S. W. High Sensitivity Sensing Membranes of High Addressable Potentiometric Sensor for Bio Material Detection. In *World Congress on Medical Physics and Biomedical Engineering 2006*; Springer: Berlin, Heidelberg, 2007; Vol. *14*, pp 1349−1352.

(28) Long, R.; Bakker, E. *Anal. Chim. Acta* **2004**, *511*, 91−95.

(29) Qin, Y.; Mi, Y. M.; Bakker, E. *Anal. Chim. Acta* **2000**, *421*, 207−220.

(30) Mi, Y. M.; Bakker, E. *Anal. Chem.* **1999**, *71*, 5279−5287.

(31) Bakker, E.; Pretsch, E. *Anal. Chem.* **1998**, *70*, 295−302.